Journal of Sound and Vibration 326 (2009) 740–752

Contents lists available at ScienceDirect

Journal of Sound and Vibration

journal homepage: www.elsevier.com/locate/jsvi

Coupled bending-torsional vibration analysis of rotor with rub and crack

Tejas H. Patel [a,b], Ashish K. Darpe [b,*]

[a] Department of Mechanical Engineering, Charotar Institute of Technology, Changa 388421, India
[b] Department of Mechanical Engineering, Indian Institute of Technology Delhi, Hauz Khas, New Delhi 110016, India

ARTICLE INFO

Article history:
Received 14 July 2008
Received in revised form
12 April 2009
Accepted 6 May 2009
Handling Editor: J. Lam
Available online 7 June 2009

ABSTRACT

Rotor–stator rub and fatigue crack of the shafts are two important rotor faults. They have detrimental effects on health and reliability of the rotating machinery. In this paper, modelling and vibration signature analysis of rotor with rotor–stator rub, transverse fatigue crack and unbalance is attempted. The rotor–stator interaction effects on the response of a rotor are investigated in the presence/absence of a transverse crack. The torsional vibrations are investigated for their sensitivity to rubbing using finite element model that also accounts for cross coupling of stiffness introduced due to crack. Due to the presence of both rotor–stator rub and transverse crack in a horizontal rotor, the system becomes highly nonlinear. The time localised rub excitations and nonlinear stiffness variation due to breathing of the crack influence the rotor response in both lateral and torsional modes and are explored extensively using Hilbert–Huang transform with the objective of unravelling some unique features of these faults that may be useful for fault identification.

1. Introduction

The present day rotors are more flexible and operate under tight clearances and harsh environment. One or more faults are likely to creep in the system under such circumstances. For example, rotor might develop contact with the stationary parts under tighter clearances or rotor could develop fatigue crack under severe thermal and mechanical stresses. Rub and crack are two important rotor faults, which could lead to catastrophic failure, if remain undetected. Rotor rubbing to stationary parts is considered as a secondary phenomenon resulting from primary cause, which perturbs the machine during normal operation and generates rotor vibrations. The sources for primary causes could be rotor unbalance, misalignment, fluid forces or some other disturbances like shaft crack. The present study is aimed to examine one such situation wherein the effect of three different disturbing functions, namely unbalance, rotor–stator rub and transverse fatigue crack is simulated together. The rotor vibration response resulting due to rotor–stator rub exhibits characteristics typical of any nonlinear system. Presence of crack in rotor system also exhibits nonlinearities. Hence, it is essential to understand exact nature of nonlinear vibration response of rotor with rub from fault diagnosis point of view and to understand its unique vibration signature. In present study, steady state vibration response of a rotor supported on simple rigid bearings is investigated using FE simulation. The study fully explores the coupling of torsional and bending vibrations introduced due to both rub and crack.

* Corresponding author.
E-mail address: akdarpe@mech.iitd.ac.in (A.K. Darpe).

0022-460X/$ - see front matter © 2009 Elsevier Ltd. All rights reserved.
doi:10.1016/j.jsv.2009.05.020

It may be noted that, it is common to study fault vibration signature in isolation from all other disturbing mechanisms. Unbalance apart, most of the past studies do not account for the presence of any other fault while investigating the vibrations related to cracked rotor or rotor rub. The actual rotor bearing system can have a varying degree of nonlinearity and could often be a multi fault system; the assumption of single fault rotor system may be an idealistic situation. For example, a rotor system can always have some amount of unbalance, misalignment in the driveline, temporary bow, etc. However, these can be within the permissible limits. It is thus important to study the effect of presence of an additional fault on the established response features of the already existing fault. In recent past, only a few research studies have addressed this issue. Bachschmid and Pennacchi [1], Platz et al. [2], and Bachschmid et al. [3] applied model based technique for multiple faults identification. Based on the signal based diagnostic approaches, Chan and Lai [4] and Darpe [5] studied the vibration response of the rotor system with crack and asymmetry faults together. They observed subharmonic resonances at $\frac{1}{2}$ and $\frac{1}{3}$ of the critical speed for the cracked shaft. Wan et al. [6] investigated vibration of a cracked rotor sliding bearing system with rotor–stator rubbing, using harmonic wavelet transform (HWT). They observed differences in wavelet time–frequency maps of cracked rotor with and without rubbing. Although, they have not separated out the distinguishing features related to crack and rubbing. Recently, Darpe et al. [7] investigated the effect of bow on the nonlinear nature of the crack response. Patel and Darpe [8] have numerically and experimentally investigated the rotor whirl characteristics of the unbalance, crack and rotor–stator rub faults. With classical Jeffcott rotor model, neglecting torsional degree of freedom, only two lateral degrees of freedom are considered for the study. Difference in whirl nature of the lateral vibration response of these faults is proposed for fault detection when these faults exist alone as well as together.

There has been extensive research on rotor–stator contact phenomenon. Depending upon system parameters and operating conditions, different types of rubbing conditions prevail. These are manifested by one or more of the physical phenomena, i.e. friction, impacting and stiffening [9]. As a result, rotor exhibits highly nonlinear and complicated vibration motion, such as periodic, quasi-periodic and chaotic vibrations with sub-synchronous and super-synchronous frequency components. Researchers have investigated rotor motion for variety of the rubbing conditions. Beatty [10] emphasised on monitoring of second and third harmonics of the synchronous frequency for the rotor rubbing. Childs [11] showed the existence of the subharmonics at $\frac{1}{3}X$ and $\frac{1}{2}X$ of rotation speed. Muszynska and Goldman [12] concluded that the vibration behaviour of such systems are characterised by regular periodic vibrations of synchronous ($1X$) and sub-synchronous ($\frac{1}{2}X$, $\frac{1}{3}X$,…) orders, as well as chaotic vibration patterns of the rotor, all accompanied by higher harmonics. Groll and Ewins [13] found subharmonic and superharmonic frequencies in the steady state vibration response due to rotor–stator interactions. Strong subharmonic measured was sometimes as low as $X/32$ and strong superharmonic measured was sometimes as high as $9X$. Sawicki et al. [14] observed subharmonic, quasi-periodic and chaotic vibrations. The $\frac{1}{2}$ and $\frac{1}{3}$ order subharmonics were related to the quadratic and cubic nonlinearity, respectively. Chu and Lu [15] carried detailed experimental work to investigate nonlinear vibrations in a rub impact rotor system. They observed very rich form of periodic and chaotic vibrations. Besides multiple harmonic components $2X$ and $3X$, sometimes $\frac{1}{2}$ and $\frac{1}{3}$ fractional harmonic components (such as $\frac{1}{2}X$, $\frac{3}{2}X$, $\frac{5}{2}X$ and $\frac{1}{3}X$, $\frac{2}{3}X$, $\frac{4}{3}X$, etc.) were present.

Apart from periodic response with subharmonic and superharmonic frequencies, rub in rotor can produce highly nonlinear vibrations, such as quasi-periodic and chaotic vibrations. Patel and Darpe [16] discussed use of spectrum cascade for identification of rub and showed existence of pseudo-resonance and backward whirling components. Choy et al. [17] investigated different regimes of rotor–casing rub, such as full rub, rigid bouncing and chaotic motion of the rotor. Li and Paidoussis [18] have shown that the vibration motion can be forward or backward whirling, depending upon the parameters. The impact behaviour could be periodic, quasi-periodic or chaotic. Chu and Zhang [19] and Sun et al. [20] studied periodic, quasi-periodic and chaotic rotor vibrations and influence of damping on chaotic behaviour. Qin et al. [21] observed grazing bifurcation and chaos in the response of rubbing rotor.

Studies on the rotor rub response are mainly done using rotor models with lateral degrees of freedom only. Effect of rotor–stator rub on the torsional response of the rotor is often neglected. Edwards et al. [22] showed the change in bifurcation behaviour as well as rotor response due to inclusion of torsional degree of freedom in the equations of motion. Al-Bedoor [23] studied the transient vibration response of the rubbing rotor. Split in lateral resonance was observed for the lateral–torsional model, which highlighted the influence of torsion on overall dynamics of the rotor system. On the other hand, issue of coupled bending-torsional vibrations is well addressed in case of cracked rotor, e.g. Papadopoulous and Dimarogonas [24], Muszynska et al. [25], Darpe et al. [26], etc. The steady state torsional response of the cracked rotor is studied and its spectral nature is established. Darpe et al. [26] discussed a comprehensive crack model in the form of stiffness matrix of the cracked finite element and highlighted the inherent coupling in lateral–longitudinal–torsional vibration response due to the presence of crack in a rotor. The paper focussed on the cracked rotor lateral vibration response in time and frequency domain to external torsional or longitudinal excitation to reveal identification features for crack diagnosis.

Higher levels of vibration due to crack in a rotor may develop rotor–stator rubbing in tight clearance situation. Both these faults (rub and crack) introduce nonlinearity in the system of equations, generating higher harmonics in the response. In such situation, it is important to understand their specific vibration signatures for unique fault identification. The primary objective of the present study is to investigate the vibration characteristics of a rotor in presence of unbalance, rotor–stator rub and transverse crack. However, the study is also involves establishing vibration features of rub+unbalance and crack+unbalance before comparing these response features in presence of both the faults in coupled vibration mode. Lateral–torsional coupled vibration is investigated with special attention to examination of the exact nature of torsional excitations of these faults (i.e. rub and crack). The present work utilises the crack model presented in Ref. [26] and

extending the rotor–stator rub model of Ref. [8] by including torsional excitation due to rubbing contact. The model of the rotor–stator system thus allows us to investigate the influence of unbalance, rotor–stator rub and crack on the coupled vibrations. Since the rub fault is highly nonlinear and transient, use of HHS is made for the study along with the conventional Fourier transform. To capture the transient response features inherent in the contact interactions in the rotor–stator rub, Hilbert–Huang transform (HHT) and associated HH spectrum is used extensively for analysis of the simulated response data. Before discussing the results, Hilbert–Huang transform is discussed in brief.

2. Hilbert–Huang transform

Earlier efforts on the rotor faults related investigations were mainly on establishing the vibration symptoms of rotor fault using conventional time-domain (i.e. vibration waveform, orbit plot, etc.) and frequency-domain (i.e. FFT) signal representation methods. However, these methods are insufficient and sometimes theoretically inappropriate for processing the signals generated by faults that generate short time transient response. This is particularly true for the highly nonlinear and transient rotor faults like rub. The conventional signal analysis methods may also be inaccurate to reveal the fault features based on any short duration transients in the coast-up response where the frequency content changes continuously. It may be noted that the rotor rub exhibits nonlinear and non-stationary vibration response even when the rotor is operating at constant rotational speed.

Realising the inability of the conventional signal processing techniques to reveal the nonlinear and non-stationary nature of the faults, researchers have recently started using advanced signal representation techniques such as wavelet map, Hilbert–Huang spectrum (HHS), etc. These techniques represent the vibration signal in the form of time–frequency–energy maps. This facilitates in detection of exact occurrence time of nonlinear event (for example, initiation of rub, subharmonic resonances for coasting up cracked rotor, etc.) and associated excitation frequencies. During the last decade or so, wavelets are increasingly used for extracting the time–frequency features of the non-stationary signals. Peng et al. [27] demonstrated the application of wavelet analysis for numerical and experimental rub signal. Like other signal processing techniques wavelet transform (WT) also suffers from certain weaknesses, mainly the leakage of energy in the neighbouring modes due to unequal time–frequency resolution defined by Heisenberg–Gabor inequality.

Huang et al. [28] presented the empirical mode decomposition (EMD) technique to decompose any complicated vibration data into finite number of intrinsic mode functions (IMF). These IMFs are complete, adaptive and almost orthogonal representation of the complex vibration signal. Recently Hilbert transform (HT) based on IMFs (also known as Hilbert–Huang transform) derived using EMD is evolved as powerful tool for analysis of nonlinear and non-stationary signal. Yu et al. [29] presented local Hilbert transform and local Hilbert marginal transform based on EMD for the fault diagnosis of roller bearings. Qi et al. [30] demonstrated the use of EMD for rubbing fault diagnosis from steady state response. Though Hilbert–Huang and wavelet transforms show time–frequency–energy distribution of the vibration signal, the former is adaptive and provides equal resolution at all frequencies and time instants, which makes use of HHT more meaningful for transient vibration signals such as rotor coast up vibration response.

Generally, frequency is defined as the number of oscillations per unit time of a physical field parameter such as displacement, current or voltage. However, for non-stationary and nonlinear signals commonly encountered in machine vibration analysis applications, this definition becomes ambiguous and loses its effectiveness over the fact that the spectral characteristics of the signals vary with time [31]. The key to the applicability of instantaneous frequency (IF) is thus to be able to decompose a signal into its individual monocomponents to which the basic definition of instantaneous frequency can be applied. Empirical mode decomposition is such a decomposition scheme through which almost orthogonal, intrinsic monocomponents can be obtained following a recursive process. Applying Hilbert transform on IMFs, one can get time–frequency–energy map, which is known as Hilbert–Huang spectrum.

The original signal can be represented as [28],

$$y(t) = \sum_{j-1}^{n} c_j + r_n \tag{1}$$

For one IMF $c_i(t)$, we can have its Hilbert transform as

$$H_i(t) = \frac{P}{\pi} \int_{-\infty}^{\infty} \frac{c_i(t')}{t - t'} \, \mathrm{d}t' \tag{2}$$

where P is Cauchy principal value.

With this definition, an analytic signal is given as

$$x_i(t) = c_i(t) + \mathrm{j}H_i(t) = a_i(t)\mathrm{e}^{\mathrm{j}\phi_i(t)} \tag{3}$$

in which

$$a_i(t) = \sqrt{[]c_i^2(t) + H_i^2(t)} \tag{4}$$

$$\phi_i(t) = \arctan \frac{H_i(t)}{c_i(t)} \tag{5}$$

One can write the instantaneous frequency as

$$\omega_i(t) = \frac{\mathrm{d}\phi_i(t)}{\mathrm{d}t} \tag{6}$$

After performing the Hilbert transform to each IMF component, the original signal can be expressed as the real part (RP) in the following form:

$$y(t) = \mathrm{RP}\sum_{i=1}^{n} a_i(t)\mathrm{e}^{\mathrm{j}\phi_i(t)} = \mathrm{RP}\sum_{i=1}^{n} a_i(t)\mathrm{e}^{\mathrm{j}\int \omega_i(t)\,\mathrm{d}t} \tag{7}$$

Here the residue r_n is left out as it is either a monotonic function or a constant. Eq. (7) gives both amplitude and frequency of each component as functions of time.

3. FE model and equations of motion

A simple rotor bearing system with a disc is modelled using Timoshenko beam elements considering all the six degrees of freedom into account (Fig. 1). Rotor–stator rub is considered at disc location, which is centrally mounted on the shaft. The rotor is modelled using 14 beam elements. The generalised FE equation of motion is given below:

$$[M]\{\ddot{q}\} + [C]\{\dot{q}\} - \omega[G]\{\dot{q}\} + [K]\{q\} = \{F\} \tag{8}$$

where $[M]$, $[C]$, $[G]$ and $[K]$ are the mass, damping, gyroscopic and stiffness matrices, respectively, $\{F\}$ is the external excitation force vector due to unbalance and rotor–stator rub, $\{q\}$ is the generalised coordinate of the system, and ω is the rotational speed.

The inertia of the disc is lumped at its corresponding degree of freedom. Rotor–stator interactions forces are considered at disc location. The crack effect in a finite element close to the disc is simulated by substituting the stiffness matrix of an uncracked Timoshenko beam element by the crack finite element.

3.1. Rotor–stator rub forces

For the rotor–stator rub, in addition to the excitation forces along normal and tangential directions, the friction torque is also acting on the disc (Fig. 1d). Rub forces are written as

$$F_N = \begin{cases} 0 & \text{for } (e_r < \delta) \\ (e_r - \delta)k_s & \text{for } (e_r \geq \delta) \end{cases}, \quad F_T = \mu F_N \quad \text{and} \quad M_t = RF_T \tag{9}$$

where F_N and F_T and are the forces along normal and tangential directions. M_t is the friction torque. $e_r = \sqrt{[]}y^2 + z^2$ is radial displacement of the rotor, δ is the clearance between rotor and stator, μ is coefficient of friction, and k_s is stator stiffness.

Using the above forces and moments, the rotor–stator rub excitation forces are obtained along all six coordinate directions as

$$\begin{Bmatrix} F_x \\ F_y \\ F_z \\ M_{\phi_x} \\ M_{\phi_y} \\ M_{\phi_z} \end{Bmatrix} = \begin{Bmatrix} 0 \\ -F_N(y/e_r) - \psi_f F_T(z/e_r) \\ -F_N(z/e_r) + \psi_f F_T(y/e_r) \\ \psi_f R F_T \\ 0 \\ 0 \end{Bmatrix} \quad \text{if } e_r \geq \delta \quad \text{or} \quad \begin{Bmatrix} F_x \\ F_y \\ F_z \\ M_{\phi_x} \\ M_{\phi_y} \\ M_{\phi_z} \end{Bmatrix} = \begin{Bmatrix} 0 \\ 0 \\ 0 \\ 0 \\ 0 \\ 0 \end{Bmatrix} \tag{10}$$

where ψ_f is the function that decides the direction of frictional forces.

$$\psi_f = \begin{cases} -1 & \text{for } \omega R + v_t > 0 \\ 0 & \text{for } \omega R + v_t = 0 \\ 1 & \text{for } \omega R + v_t < 0 \end{cases} \quad \text{and} \quad v_t = \dot{Z}\left(\frac{Y}{e}\right) - \dot{Y}\left(\frac{Z}{e}\right) \tag{11}$$

where R is the disc radius and v_t is the tangential velocity at disc location.

It may be noted that the rub forces are included in the generalised force vector $\{F\}$ of Eq. (8) and should be applied at particular degrees of freedom corresponding to the disc location.

3.2. Stiffness matrix of crack element

Detailed derivation of the stiffness matrix of the crack element is presented in Ref. [26]; however, it is discussed briefly here for the sake of completeness. The stiffness matrix of the crack element is found out from the flexibility coefficients. The flexibility coefficients can be found using Castingliano's theorem using the strain energy of the cracked element. Consider a rotor segment containing a transverse surface crack of depth a as shown in Fig. 1(a). Let the shaft element be of

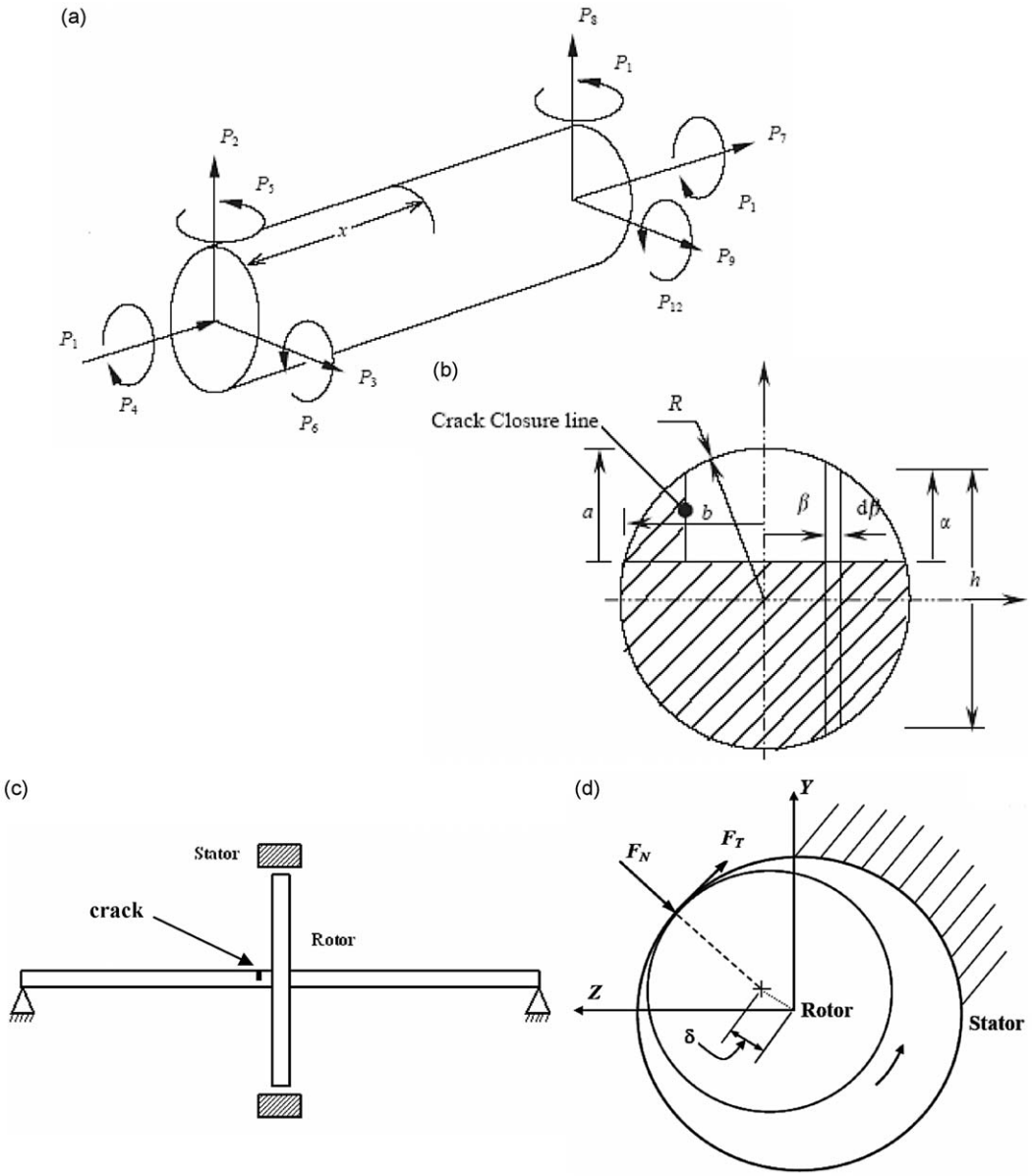

Fig. 1. (a) Crack finite element, (b) crack cross section, (c) schematic of rotor–stator system and (d) rotor–stator rub contact.

diameter D and length l. The element is under the action of shear forces P_2, P_3 and P_8, P_9, bending moment P_5, P_6 and P_{11}, P_{12}, axial forces P_1 and P_7 and torsional moments P_4 and P_{10}. The crack is situated at a distance x from left end of the element.

The strain energy of the shaft element in presence of crack can be found by using the strain energies of the uncracked shaft element and the additional strain energy due to the presence of crack are found. Castingliano's theorem may then be used to obtain the displacement and further differentiation with forces gives the flexibility elements as derived in detail by [26] and arranged in the matrix form as

$$G = \begin{bmatrix} g_{11} & g_{12} & g_{13} & g_{14} & g_{15} & g_{16} \\ g_{21} & g_{22} & g_{23} & g_{24} & g_{25} & g_{26} \\ g_{31} & g_{32} & g_{33} & g_{34} & g_{35} & g_{36} \\ g_{41} & g_{42} & g_{43} & g_{44} & g_{45} & g_{46} \\ g_{51} & g_{52} & g_{53} & g_{54} & g_{55} & g_{56} \\ g_{61} & g_{62} & g_{63} & g_{64} & g_{65} & g_{66} \end{bmatrix}$$

where

$$g_{11}=\frac{l}{AE}+\int_A\frac{2\alpha F_1^2}{\pi ER^4}\,dA,\quad g_{22}=\frac{\alpha_s l}{GA}+\frac{l^3}{3EI}+\int_A\left[\frac{2k^2\alpha F_{II}^2}{\pi ER^4}+\frac{8x^2h^2\alpha F_2^2}{\pi ER^8}\right]dA$$

$$g_{33}=\frac{\alpha_s l}{GA}+\frac{l^3}{3EI}+\int_A\left[\frac{32x^2\beta^2\alpha F_1^2}{\pi ER^8}+\frac{2mk^2\alpha F_{III}^2}{\pi ER^4}\right]dA$$

$$g_{44}=\frac{l}{GI_0}+\int_A\left[\frac{8\beta^2\alpha F_{II}^2}{\pi ER^8}+\frac{2mh^2\alpha F_{III}^2}{\pi ER^4}\right]dA,\quad g_{55}=\frac{l}{EI}+\int_A\frac{32\beta^2\alpha F_1^2}{\pi ER^8}\,dA$$

$$g_{66}=\frac{l}{EI}+\int_A\frac{8h^2\alpha F_2^2}{\pi ER^8}\,dA,\quad g_{12}=g_{21}=\int_A\frac{4xh\alpha F_1F_2}{\pi ER^6}\,dA$$

$$g_{13}=g_{31}=\int_A\frac{8x\beta\alpha F_1^2}{\pi ER^6}\,dA,\quad g_{15}=g_{51}=\int_A\frac{8\beta\alpha F_1^2}{\pi ER^6}\,dA$$

$$g_{16}=g_{61}=-\int_A\frac{4h\alpha F_1F_2}{\pi ER^6}\,dA,\quad g_{23}=g_{32}=\int_A\frac{16x^2h\beta\alpha F_1F_2}{\pi ER^8}\,dA$$

$$g_{24}=g_{42}=\int_A\frac{4k\beta\alpha F_{II}^2}{\pi ER^6}\,dA,\quad g_{34}=g_{43}=\int_A\frac{2mkh\alpha F_{III}^2}{\pi ER^6}\,dA$$

$$g_{25}=g_{52}=\int_A\frac{16xh\beta\alpha F_1F_2}{\pi ER^8}\,dA,\quad g_{35}=g_{53}=\frac{l^2}{2EI}+\int_A\frac{32x\beta^2\alpha F_1^2}{\pi ER^8}\,dA$$

$$g_{26}=g_{62}=-\frac{l^2}{2EI}-\int_A\frac{8xh^2\alpha F_2^2}{\pi ER^8}\,dA,\quad g_{56}=g_{65}=-\int_A\frac{16h\beta\alpha F_1F_2}{\pi ER^8}\,dA \tag{12}$$

where

$$F_1=\sqrt{[]}\frac{2\alpha'}{\pi\alpha}\tan\left(\frac{\pi\alpha}{2\alpha'}\right)\frac{0.752+2.02(\alpha/\alpha')+0.37\left[1-\sin(\pi\alpha/2\alpha')\right]^3}{\cos(\pi\alpha/2\alpha')}$$

$$F_2=\sqrt{[]}\frac{2\alpha'}{\pi\alpha}\tan\left(\frac{\pi\alpha}{2\alpha'}\right)\frac{0.923+0.199\left[1-\sin(\pi\alpha/2\alpha')\right]^4}{\cos(\pi\alpha/2\alpha')}$$

$$F_{II}=\frac{1.122-0.561(\alpha/\alpha')+0.085(\alpha/\alpha')^2+0.18(\alpha/\alpha')^3}{\sqrt{[]}1-(\alpha/\alpha')}$$

$$F_{III}=\sqrt{[]}\frac{2\alpha'}{\pi\alpha}\tan\left(\frac{\pi\alpha}{2\alpha'}\right) \tag{13}$$

The flexibility matrix is now used to find the stiffness matrix using the transformation matrix $[T]$ considering static equilibrium of the finite element.

$$\{q_{1-12}\}^{\mathrm{T}}=[T]\{q_{1-6}\}^{\mathrm{T}} \tag{14}$$

where the transformation matrix is given by

$$[T]^{\mathrm{T}}=\begin{bmatrix}1&0&0&0&0&0&-1&0&0&0&0&0\\0&1&0&0&0&0&0&-1&0&0&0&l\\0&0&1&0&0&0&0&0&-1&0&-l&0\\0&0&0&1&0&0&0&0&0&-1&0&0\\0&0&0&0&1&0&0&0&0&0&-1&0\\0&0&0&0&0&1&0&0&0&0&0&-1\end{bmatrix} \tag{15}$$

Thus, the stiffness matrix of the cracked element is written as

$$[K]^c=[T][G]^{-1}[T]^{\mathrm{T}} \tag{16}$$

The above stiffness matrix of crack element is evaluated by finding the integral values of the expressions in Eq. (12). The limits of the integration depend on the open/close area of the crack, which is found using the sign of the overall stress

intensity factor (SIF) [26]. The negative sign of SIF indicates compressive stress and the closed crack condition and positive sign indicates tensile state of stress and open crack condition. Accordingly, depending on the instantaneous state of forces acting on the crack element, the SIF is influenced, which influences the stiffness matrix. The stiffness matrix calculated at any instant is used in the equations of motion along with the rub forces (Eq. (10)) at that moment to evaluate the response of the rotor bearing system.

4. Coupled vibration analysis using IF and HHS plot

System parameters considered in present study are as follows: disc mass, $m = 6$ kg; disc area moment of inertia, $I_d = 12.14\text{E}{-}03$ mm^4; shaft diameter, $d = 25$ mm; shaft length, $L = 0.7$ m; stator stiffness, $K_s = 350 \times 10^{+6}$ N/m; coefficient of friction, $\mu = 0.2$ and unbalance eccentricity, $\varepsilon = 1.0597 \times 10^{-5}$ m. To simulate rub condition, rotor–stator clearance $= 1.07 \times 10^{-4}$ m is taken. Vibration responses are first studied for rub and crack faults independently in presence of unbalance and then when they exist together with unbalance. Crack depth of $a/d = 0.30$ is considered for the cracked rotor. Solution to the equations of motion is obtained numerically, using Newmark-beta method. Vibration response is calculated with sufficiently small time step of 1/50th the time required for one degree of shaft rotation. However, the vibration data is stored only after one degree of shaft rotation. The rotational speed considered for the study is one third of the first bending natural frequency (14.64 Hz) that gives the data sampling frequency of 5271 Hz. The torsional natural frequency of the uncracked rotor is 95.5 Hz. Investigations are first carried out for the cases (i.e. uncracked and cracked rotors) without rotor–stator rub, followed by the vibration analysis for the cases of uncracked and cracked rotors with rotor–stator rub. This allows us to investigate the influence of presence of crack on the robustness of the rub vibration signature. It may be noted that in [8], the authors have reported the changes in the whirl characteristics (backward/forward) due to simultaneous presence of these faults (i.e. unbalance, crack and rub).

The unbalance vibration response of the uncracked rotor without rub is shown in Fig. 2 in the form of vibration waveform, FFT, Instantaneous frequency (IF) plot and Hilbert Huang spectrum (HHS). It may be noted that the vibration data of four complete cycles of rotor rotation is displayed in the respective figures for all the cases discussed in the paper. The vertical vibration response is synchronous with rotational speed and hence FFT shows only one peak at 14.64 Hz (i.e. rotational frequency) in the Fourier spectrum. The IF plot shows a horizontal line that represents the instantaneous frequency of 14.64 Hz. This line remains horizontal without any perturbation throughout the four cycles of rotation. In HHS, there is one dark line parallel to abscissa (i.e. angle of rotation) at 0.0028 value of normalised frequency. This corresponds to actual frequency of 14.64 Hz (i.e. 0.0028 × sampling frequency). It may be recalled from Section 2 that the HHS is the time–frequency–amplitude representation of the signal in the form of 2D map. Frequencies with higher level of energy are shown with darker colour. The HHT of the unbalance response of uncracked rotor in Fig. 2 thus indicates same energy level throughout. Although the IF plot is similar to HHS, it does not include the energy (i.e. amplitude) information. In other words, the IF plot indicates the presence/absence of frequency, the HHS indicates the level of energy (given by darkness of the point in the map) associated with a particular frequency component (indicated by the position along the ordinate) at any instant of time (given by location along abscissa).

Fig. 3 shows the vertical vibration response of the cracked rotor in the presence of unbalance. The added flexibility due to crack increases the overall vibration level compared to the uncracked rotor. The FFT plot indicates response with three distinct frequencies, i.e. 1*X*, 2*X* and 3*X*. However, the IF plot and HHS show only two intrinsic mode functions, which are varying with time, indicating the change in the frequency composition of the signal with shaft rotation angle. The mean in the frequency variations are, respectively, 0.0028 (14.64 Hz, i.e. rotational frequency) and 0.083 (43.92 Hz, i.e. bending natural frequency) for the two monocomponents. This signifies that the crack excitation frequencies are not pure "harmonics" [32]. It may be noted that a pure harmonic frequency gets represented in the form of a horizontal line in the HHS as seen from the HHS for the uncracked rotor without rub (Fig. 2). Yang and Suh [33] have related this fluctuation in frequency to the opening and closing of the crack with shaft rotation. In addition to generating the higher harmonics (2*X*, 3*X*) in the FFT, the crack also influences 1*X* response. Hence, the monocomponent corresponding to this frequency also experiences variation and hence is not a straight horizontal line in contrast to the case of pure unbalance.

The torsional vibration response of the cracked rotor is shown (Fig. 4) for rotor speed, $\omega = 14.64$ Hz. The FFT shows vibrations with mainly 1*X* and 2*X* frequency orders with weak higher harmonics. Again, these frequencies are not constant with shaft rotation angle, as indicated from HHS of Fig. 4. It can be seen that the IMFs with higher order frequencies experience largest variation. The variation of the frequencies suggests that all the frequencies indicated by FFT plot may not be present in the response at all time. The IF plot of torsional vibration of the cracked rotor (Fig. 4) shows higher value of the excitation frequency (up to 2500 Hz) for a short duration during a rotation. It may be recalled that the IF plot is nothing but a HHS minus energy (amplitude) dimension. The higher order frequencies although represented in the IF plot could be of importance if they carry enough energy. However, it may be noted from the corresponding HHS in Fig. 4 that the highest noticeable frequency is 0.03 (158 Hz).

Fig. 5 shows vertical vibration response of the uncracked rotor with rotor–stator rub. The FFT plot shows $\frac{1}{2}X$ order harmonics in the vibration response. From FFT plot and vibration waveform, it may be noted that the vibration motion is period-2 motion, i.e. motion is exactly repeated after two cycles of rotation. From the vertical vibration signal of Fig. 5, the rotor–stator contact phenomenon is evident. It can be seen that the rotor comes in contact with stator for only fraction of

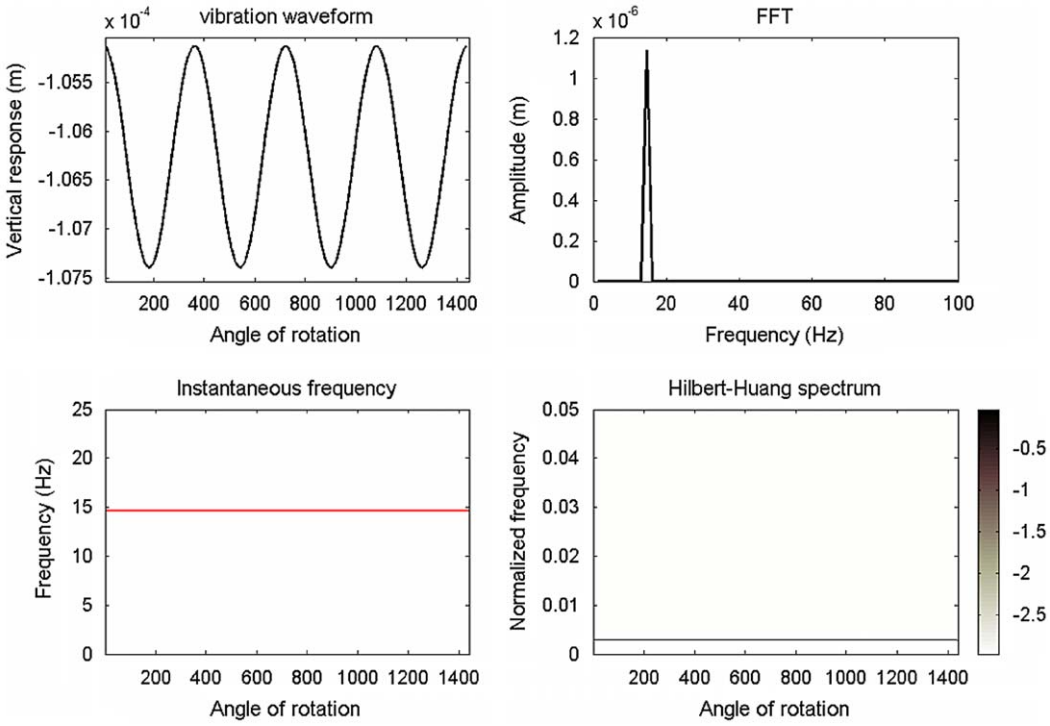

Fig. 2. Waveform, FFT, IF plot and HHS of unbalance vibration response of uncracked rotor without rub.

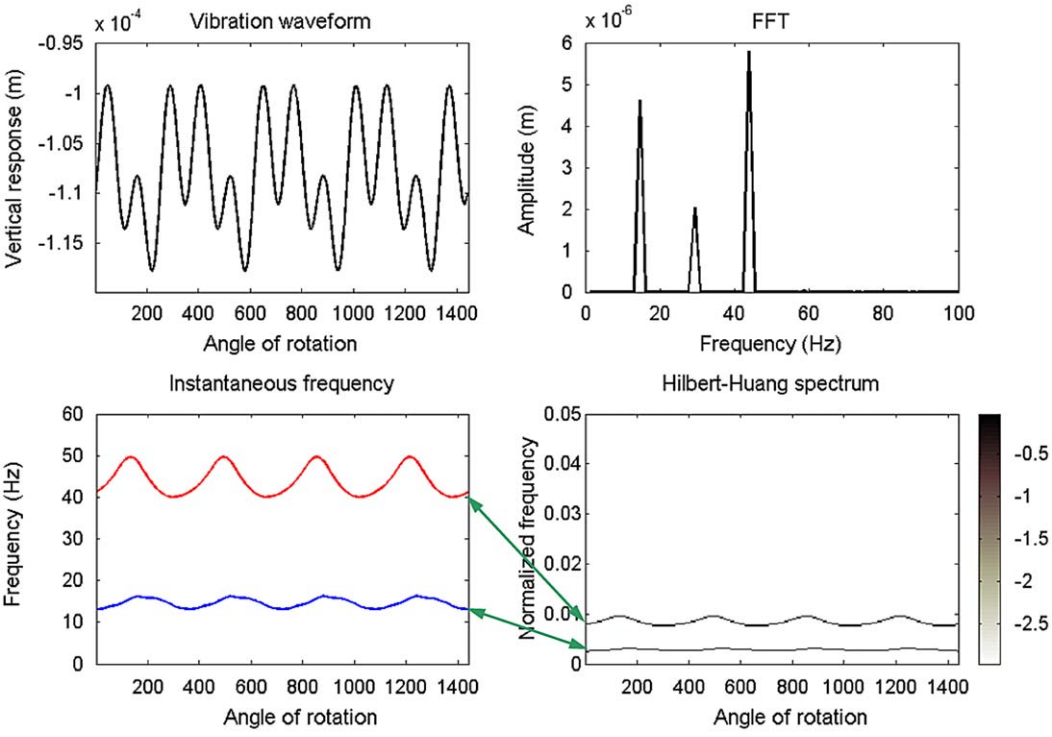

Fig. 3. Waveform, FFT, IF plot and HHS of vertical vibration response of cracked rotor without rub.

cycle time. In the present case, the rotor interacts with stator during roughly 130–230°, 490–590°, 850–950° and 1210–1310° angle of shaft rotation. Higher frequencies are excited during this period of rotor–stator contact, as revealed from IF and HHS plots (Fig. 5). However, once the rotor–stator contact breaks, the vibration signal becomes harmonic with

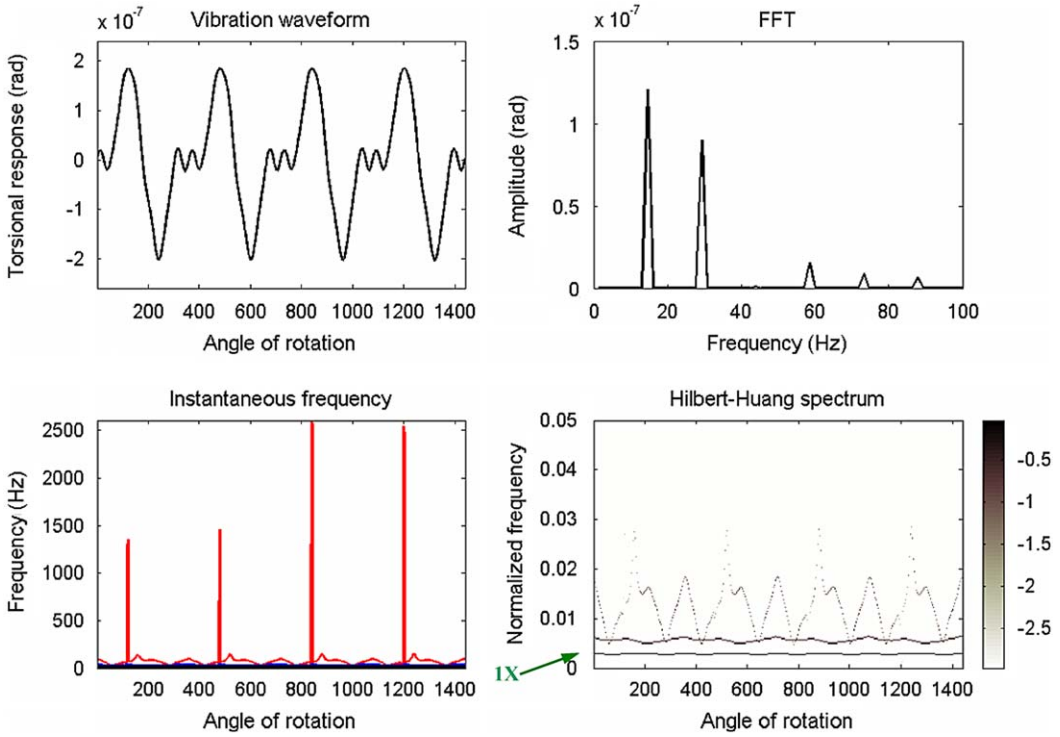

Fig. 4. Waveform, FFT, IF plot and HHS of torsional vibration response of cracked rotor without rub.

rotation frequency and higher order frequencies diminish. It is important to compare the HHT of uncracked rotor rub response (Fig. 5) with the cracked rotor without rub response (Fig. 3). It is observed that the repeated occurrence of higher order spectral components with abrupt variations in them with shaft rotation is due to rotor–stator rubbing. This feature is not observed in cracked rotor response without rub (Fig. 3) and hence can be used for rub diagnosis.

In general, interaction of rotor to stator is a complex and involves phenomena [9,16,17] like impacting, friction, stiffening, etc. Depending upon the rotor configuration and system parameters, one or more of the above mechanisms govern the rotor response (i.e. periodic, quasi-periodic and chaotic) as well its whirl character (forward or backward). Furthermore, the rotor–stator rub can be intermittent/partial or full; depending on the time for which the rotor remains in contact with stator during a rotation. The full rub is the state of rotor motion where the rotor remains in continuous contact with the stator, which leads to backward whirling synchronous motion. However, in practice, the contacting material often wears out at rubbing locations and rotor returns back either to intermittent rubbing state or to no-rub state. Intermittent rub is thus more common than the full rub. The rotor with intermittent rub mainly excites higher harmonics irrespective of the type of response it exhibit (i.e. periodic, quasi-periodic and chaotic). These higher order spectral components are evident in the response as shown in Fig. 5 and can be expected in many practical situations.

The torsional vibration response of uncracked rotor with rub is shown in Fig. 6. The nonstationary feature of the rub signal is also observed here. The FFT shows strong amplitudes of vibration at 95.16 Hz (i.e. $\frac{13}{2}X$), with side bands separated by $\frac{1}{2}X$. It may be noted that the torsional natural frequency of the rotor is 95.5 Hz, and as a result 13th harmonics of $\frac{1}{2}X$ experiences higher vibration level. When rub occurs, frequencies up to 240 Hz are excited (as noted from the HHS). Since rotor rub is the only source of excitation for setting up torsional mode vibration, once the rotor leaves the contact with stator, the vibrations at torsional natural frequency are induced in the system. This is clearly evident from the IF and HHS plots. It may be noted that the rotor–stator rub does not occur during 230–490°, 590–850° and 950–1210° angles of shaft rotation. The IF and HHS plots for these periods of shaft rotation show torsional natural frequency as the only significant frequency component of the torsional response (Fig. 6). Due to the existing damping in the system, the torsional vibrations damp out with time.

It may be further noticed from the time domain signal that the torsional vibrations are modulated and this is also observed from the side bands of $\frac{1}{2}X$ order frequency about the $\frac{13}{2}X$ frequency (95.16 Hz) in the FFT plot in Fig. 6. This modulation phenomenon is effectively captured in the HHS. The noticeable modulation of torsional natural frequency in the torsional response is a strong identifying feature of rub and hence recommended for its detection. It may be noted that this feature is not observed for other faults, for example torsional response of cracked rotor shows mainly $1X$ and $2X$ vibrations with variation in frequency. The features observed in the HHS are unique fault features for rub and are proposed for its identification.

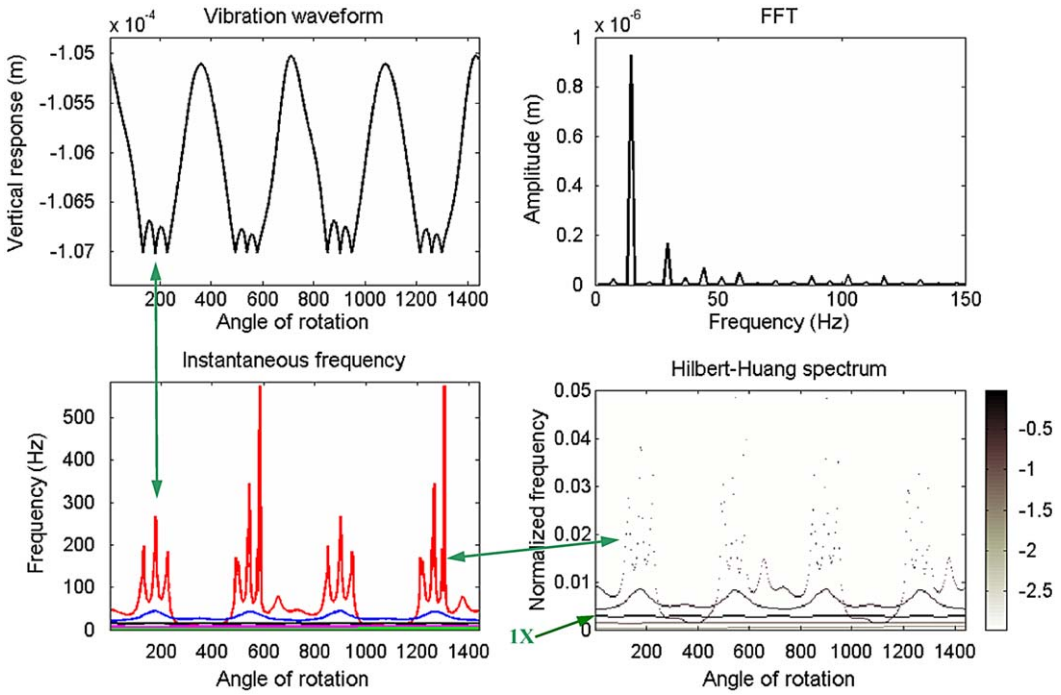

Fig. 5. Waveform, FFT, IF plot and HHS of vertical vibration response of uncracked rotor with rub.

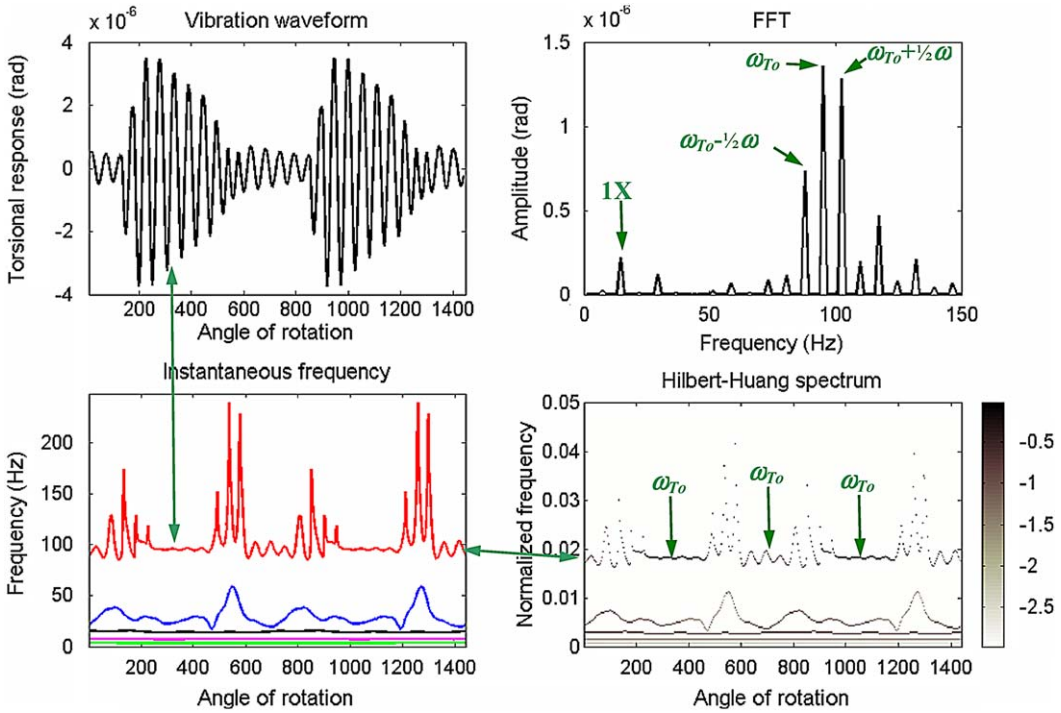

Fig. 6. Waveform, FFT, IF plot and HHS of torsional vibration response of uncracked rotor with rub.

Vertical and torsional vibration responses of the cracked rotor in presence of rotor–stator rub is now discussed. The lateral and torsional vibration response for this multi-faults case (unbalance+rub+crack) are examined and compared with the individual fault features observed from Figs. 2–6. Fig. 7 shows vertical vibration response of the cracked rotor with rub. It may be noted that the rotor–stator clearance is the control parameter to simulate the rotor–stator rub. To introduce

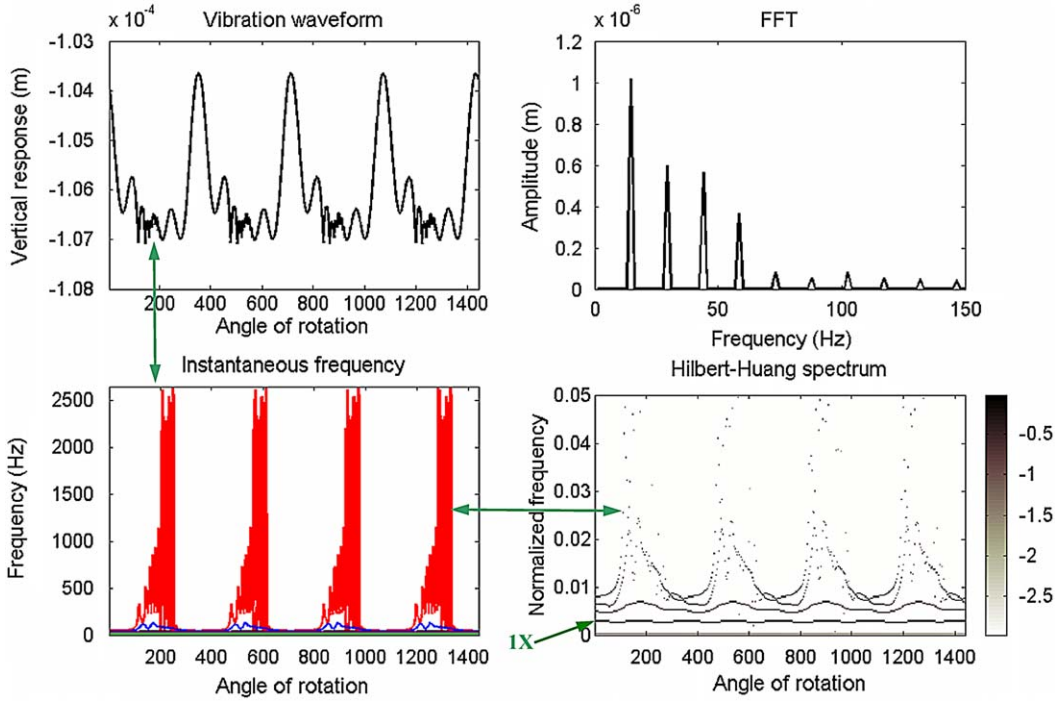

Fig. 7. Waveform, FFT, IF plot and HHS of vertical vibration response of cracked rotor with rub.

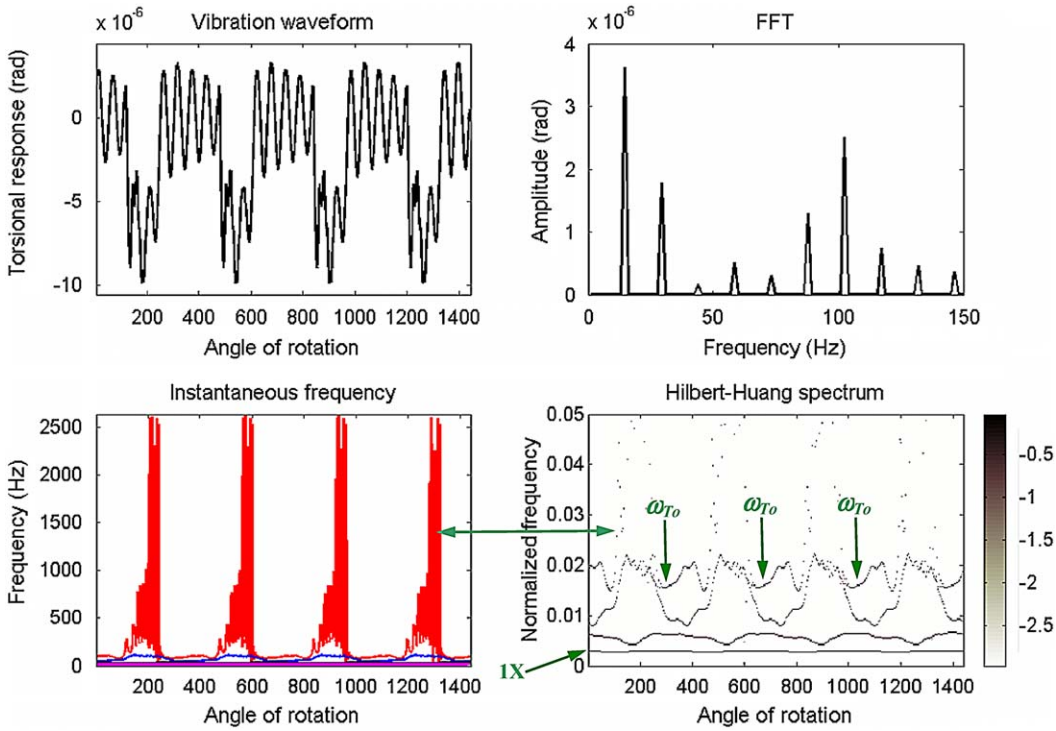

Fig. 8. Waveform, FFT, IF plot and HHS of torsional vibration response of cracked rotor with rub.

rotor–stator rub effect in uncracked and cracked rotors; the rotor–stator clearance is considered to be less than the total rotor radial excursion due to only unbalance excitation (without rub). In this way the rotor radial movement is restricted in the cases of rotor–stator rub, which is reflected in the reduced rotor response in lateral directions in Figs. 5 and 7 compared to the case of cracked rotor without rub (Fig. 3).

From the vibration waveform and FFT plot (Fig. 7), it may be noted that the harmonics of 1*X* order exists in the response. The IF plot and HHS show that the higher frequencies gets excited as rub takes place. These frequencies disappear once the rotor loses the contact. It may be noted that due to higher level of vibrations due to presence of crack, the rotor in this case interacts more with stator. The rub occurs for 60–290°, 420–650°, 780–1010°, and 1140–1370° of shaft rotation angular positions. The IF plot and HHS, correspondingly show higher harmonics in the lateral vibrations, with fluctuation in the excitation frequencies, which is a typical rub feature. The higher frequencies disappear when there is no rub, for example at 290–420°, 650–780° and 1010–1140° of shaft rotation.

Fig. 8 shows torsional vibration response of the cracked rotor with rub. FFT of the torsional vibrations shows strong 1*X* and 7*X* (102.5 Hz) frequency components. It may be noted that since response has harmonics of 1*X* order, the 7*X* is nearer to the torsional natural frequency. Presence of strong 1*X* is attributed to crack, since rub in uncracked rotor did not show significant 1*X* component as noted from the relative darkness of 1*X* curve in the HHS of Figs. 6 and 8. Presence of the torsional natural frequency is due to rub only, since other rotor faults do not excite torsional natural frequency as strongly as rub does since there is a direct transient excitation in torsional mode. From the angular location values mentioned, for which the rotor contacts the stator, it may be noted that the contact vanishes for 290–420°, 650–780° and 1010–1140° shaft rotation angles. The IF plot and HHS reveal strong torsional natural frequency component during these instances of the shaft rotation. For other angles, there is modulation of torsional natural frequency by 1*X* (i.e. modulating frequency). The modulation phenomenon of torsional natural frequency is a typical indication of rub. In case of uncracked rotor with rub, the modulation of frequency close to torsional natural frequency is by a $\frac{1}{2}X$ frequency component, whereas in the case of cracked rotor, the modulation is by 1*X*. In general, it may be noticed that when crack and rub coexists in rotor system, vibration response exhibit features specific to both the faults. The amplitude of torsional vibration is rather low in the cases discussed above. In general, the vibration amplitudes are sensitive to crack depth, so the torsional response could increase for deeper crack. It may also be possible to measure lower level torsional vibrations using laser based instruments.

5. Concluding remarks

In this paper, steady state coupled lateral–torsional vibration response for crack and rub faults are investigated using FE model. The lateral–torsional coupling is studied and vibration responses are analysed using HHT. The study brings out the nonlinear and non-harmonic nature of the spectral components for the rotor faults. The nonlinear dynamic response due to rotor–stator interaction that appears in vibration waveform is also revealed by HHT, with complete information in the form of time, frequency and associated energy. In this way, the non-stationary nature of the rotor–stator contact is accurately captured in HHS. Distinguishing features between rub and crack established earlier in [8] for lateral vibration response using full spectrum plots are augmented with torsional vibration features investigated here. The torsional vibration response features form additional information to distinguish between crack and rub faults. The torsional response of the cracked rotor is strong in 1*X* and 2*X* frequencies. The higher order frequencies are relatively weak. The rub torsional signal indicates that the vibrations are strong at torsional natural frequency modulated by $\frac{1}{2}X$. It may be noted that, this is a unique rub feature, and should be used for rub diagnosis. Torsional response of cracked rotor in presence of rub exhibits strong vibrations at 1*X* as well as at torsional natural frequency. The presence of these frequencies along with the modulation of the torsional natural frequency by the lowest frequency order present, identifies the simultaneous presence of crack and rubs faults.

References

[1] N. Bachschmid, P. Pennacchi, Model based malfunction identification from bearing measurements, *Proceedings of Seventh International IMechE Conference on Vibration in Rotating Machinery*, Nottingham, 2000, pp. 571–580.
[2] R. Platz, R. Markert, M. Seidler, Validation of online diagnostics of malfunctions in rotor systems, *Proceedings of Seventh International IMechE Conference on Vibration in Rotating Machinery*, Nottingham, 2000, pp. 581–590.
[3] N. Bachschmid, P. Pennacchi, A. Vania, Identification of multiple faults in rotor systems, *Journal of Sound and Vibration* 254 (2002) 327–366.
[4] R.K. Chan, T.C. Lai, Digital simulation of a rotating shaft with a transverse crack, *Applied Mathematical Modelling* 19 (1995) 411–420.
[5] A.K. Darpe, Dynamics of Cracked Rotor, PhD Thesis, Department of Mechanical Engineering, IIT Delhi, New Delhi, 2000.
[6] F. Wan, Q. Xu, S. Li, Vibration analysis of cracked rotor sliding bearing system with rotor–stator rubbing by harmonic wavelet transform, *Journal of Sound and Vibration* 271 (2004) 507–518.
[7] A.K. Darpe, K. Gupta, A. Chawla, Dynamics of bowed rotor with transverse surface crack, *Journal of Sound and Vibration* 296 (2006) 429–445.
[8] T.H. Patel, A.K. Darpe, Vibration response of a cracked rotor in presence of rotor–stator rub, *Journal of Sound and Vibration* 317 (2008) 841–865.
[9] A. Muszynska, *Rotor-to-Stationary Part Rubbing Contact in Rotating Machinery, Rotordynamics*, CRC Press, Taylor & Francis, Boca Raton, 2005, pp. 555–710.
[10] R.F. Beatty, Differentiating rotor response due to radial rubbing, *Journal of Vibration and Acoustics, Stress and Reliability in Design* 107 (1985) 151–160.
[11] D.W. Childs, Fractional-frequency rotor motion due to non-symmetric clearance effects, *Journal of Engineering Power* 104 (1982) 536–541.
[12] A. Muszynska, P. Goldman, Chaotic responses of unbalanced rotor-bearing-stator systems with looseness or rubs, *Chaos, Solutions and Fractals* 5 (1995) 1683–1704.
[13] G.V. Groll, D.J. Ewins, A mechanism of low sub-harmonic response in rotor/stator contact—measurements and simulations, *Journal of Vibration and Acoustics* 124 (2002) 350–358.
[14] J.T. Sawicki, J. Padovan, R. Al-Khatib, The dynamics of rotor with rubbing, *International Journal of Rotating Machinery* 5 (1999) 295–304.
[15] F. Chu, W. Lu, Experimental observation of nonlinear vibrations in a rub-impact rotor system, *Journal of Sound and Vibration* 283 (2005) 621–643.
[16] T.H. Patel, A.K. Darpe, Use of full spectrum cascade for rotor rub identification, *Advances in Vibration Engineering* 8 (2009) 1–13.
[17] F.K. Choy, J. Padovan, J.C. Yu, Full rubs, bouncing and quasi chaotic orbits in rotating equipments, *Journal of Franklin Institute* 327 (1990) 25–41.
[18] G. Li, M. Paidoussis, Impact phenomenon of rotor casing dynamical system, *Nonlinear Dynamics* 5 (1994) 53–70.

[19] F. Chu, Z. Zhang, Periodic, quasi-periodic and chaotic vibrations of a rub impact rotor system supported on oil film bearings, *International Journal of Engineering Science* 35 (1997) 963–973.
[20] Z. Sun, J. Xu, T. Zhou, Analysis of complicated characteristics of high speed rotor system with rub-impact, *Mechanism and Machine Theory* 327 (2002) 659–672.
[21] W. Qin, H. Su, Y. Yang, Grazing bifurcation and chaos in response of rubbing rotor, *Chaos, Solutions and Fractals* 37 (2008) 166–174.
[22] S. Edwards, A.W. Lees, M.I. Friswell, The influence of torsion on rotor/stator contact in rotating machinery, *Journal of Sound and Vibration* 225 (1999) 767–778.
[23] B. Al-Bedoor, Transient torsional and lateral vibration of unbalanced rotors with rotor-to-stator rubbing, *Journal of Sound and Vibration* 229 (2000) 627–645.
[24] C.A. Papadopoulous, A.D. Dimarogonas, Coupled vibrations of a cracked shaft, *Journal of Vibration and Acoustics* 114 (1992) 461–467.
[25] A. Muszynska, P. Goldman, D.E. Bently, Torsional/lateral vibration cross coupled responses due to shaft anisotropy: a new tool in shaft crack detection, *Proceedings of IMechE, Journal of Mechanical Engineers* (1992) 257–262.
[26] A.K. Darpe, K. Gupta, A. Chawla, Coupled bending, longitudinal and torsional vibrations of a cracked rotor, *Journal of Sound and Vibration* 269 (2004) 33–60.
[27] Z. Peng, P.W. Tse, F. Chu, An improved Hilbert–Huang transform and its application in vibration signal analysis, *Journal of Sound and Vibration* 286 (2005) 187–205.
[28] N.E. Huang, et al., The empirical mode decomposition and the Hilbert spectrum for nonlinear and non-stationary time series analysis, *Proceedings of the Royal Society of London* 454 (1998) 903–995.
[29] D. Yu, J. Cheng, Y. Yang, Application of EMD method and Hilbert spectrum to the fault diagnosis of roller bearings, *Mechanical Systems and Signal Processing* 19 (2005) 259–270.
[30] K. Qi, Z. He, Y. Zi, Cosine window-based boundary processing method for EMD and its application in rubbing fault diagnosis, *Mechanical Systems and Signal Processing* 21 (2007) 2750–2760.
[31] B. Boashash, Estimating and interpreting the instantaneous frequency of a signal—part I: fundamentals, *Proceedings of IEEE* 80 (1992) 520–538.
[32] D. Guo, Z. Peng, Vibration analysis of a cracked rotor using Hilbert–Huang transform, *Mechanical Systems and Signal Processing* 21 (2007) 3030–3041.
[33] B. Yang, C. Suh, Interpretation of crack induced rotor nonlinear response using instantaneous frequency, *Mechanical Systems and Signal Processing* 18 (2004) 491–513.